Smith ScholarWorks

Geosciences: Faculty Publications

Geosciences

1-1-2019

New Source-to-Sink Approach in an Arctic Catchment Based on Hyperspectral Core-Logging (Lake Linné, Svalbard)

Antonin Van Exem
CNRS Centre National de la Recherche Scientifique

Maxime Debret
CNRS Centre National de la Recherche Scientifique

Yoann Copard
CNRS Centre National de la Recherche Scientifique

Charles Verpoorter
Université du Littoral Côte d'Opale

Gregory De Wet
University of Colorado Boulder, gdewet@smith.edu

See next page for additional authors

Follow this and additional works at: https://scholarworks.smith.edu/geo_facpubs

Part of the Geology Commons

Recommended Citation

Van Exem, Antonin; Debret, Maxime; Copard, Yoann; Verpoorter, Charles; De Wet, Gregory; Lecoq, Nicolas; Sorrel, Philippe; Werner, Alan; Roof, Steven; Laignel, Benoit; and Retelle, Michael, "New Source-to-Sink Approach in an Arctic Catchment Based on Hyperspectral Core-Logging (Lake Linné, Svalbard)" (2019). Geosciences: Faculty Publications, Smith College, Northampton, MA.
https://scholarworks.smith.edu/geo_facpubs/148

This Article has been accepted for inclusion in Geosciences: Faculty Publications by an authorized administrator of Smith ScholarWorks. For more information, please contact scholarworks@smith.edu

Authors
Antonin Van Exem, Maxime Debret, Yoann Copard, Charles Verpoorter, Gregory De Wet, Nicolas Lecoq, Philippe Sorrel, Alan Werner, Steven Roof, Benoit Laignel, and Michael Retelle

This article is available at Smith ScholarWorks: https://scholarworks.smith.edu/geo_facpubs/148

Version of Record: https://www.sciencedirect.com/science/article/pii/S0277379118303998
Manuscript_07f0d00422971289ce77ddaced7f0e4e

New source-to-sink approach in an arctic catchment based on hyperspectral core-logging (Lake Linné, Svalbard)

Antonin Van Exem[1], Maxime Debret[1], Yoann Copard[1], Charles Verpoorter[2], Gregory De Wet[3], Nicolas Lecoq[1], Philippe Sorrel[4], Alan Werner[5], Steven Roof[6], Benoit Laignel[1] and Michael Retelle[7]

(1) Normandie Univ, UNIROUEN, UNICAEN, CNRS, M2C, 76000 Rouen, France,
(2) Université du Littoral Côte d'Opale, Université de Lille, CNRS UMR 8187, LOG, Wimereux, France,
(3) University of Colorado, Boulder, Boulder CO, United States
(4) Université de Lyon, UCBL, ENSL, CNRS, LGL-TPE, 69622 Villeurbanne, France
(5) Mt. Holyoke College, Dept. of Geology, South Hadley, MA, USA,
(6) Hampshire College, Amherst, MA, USA,
(7) Bates College, Lewiston, ME, USA

Key-words: Paleolimnology; optical methods; lamina; Svalbard; data treatment; Holocene, total organic carbon

1 Introduction

The Arctic region is heavily affected by the impacts of climate change (e.g. Swart 2017). Notably, the retreat of numerous glaciers is clearly observed during the last century, which coincides with greatly increased anthropogenic greenhouse gas emissions (IPCC, 2013). However, temporal variability in glacial activity prior to the instrumental record is still debated by paleoclimatologists. Prior to the era of direct observations, one possible way to track glacial oscillations and also variation in hydro-sedimentary transfer, both potentially caused by climate change, is to study the origin of sediments deposited in proglacial lakes (e.g. Nesje *et al.*, 2001; de Wet *et al.*, 2017; Briner *et al.*, 2016; Pages 2K Consortium, 2013). Sedimentary source identification is mainly based on experimental and destructive methods (lithogenic radionuclides, geochemistry, particle size and shape) at low resolution (i.e. low

© 2018 published by Elsevier. This manuscript is made available under the Elsevier user license
https://www.elsevier.com/open-access/userlicense/1.0/

sampling interval) (Koiter *et al.*, 2013; Owens *et al.*, 2016; Resentini *et al.*, 2016). However, the use of such low-resolution methods is strongly limited as some lacustrine deposits are finely laminated and may require high-resolution analyses to accurately characterise sedimentary changes potentially linked to climate change. In this context, the "source-to-sink" approach, which entails the comparison of different sources in the lake catchment with sediments stored in lacustrine deposits, is highly useful (Milliman and Syvitski, 1992; Walsh *et al.*, 2016). Currently, these methods generally consist of the study of (i) mineral properties (e.g. magnetism, Horng and Huh 2011, Sandgren and Snowball (2001)), mineral geochemistry (e.g. Revel-Rolland *et al.*, 2005; Bonneau *et al.*, 2016) and (ii) the organic moiety (biomarkers, thermal stability, e.g. Leithold *et al.*, 2016). All these techniques are destructive, may consume a large amount of material, and are time consuming. These limitations make it difficult to study several cores from the same lake, which is essential to validate the significance of the scientific findings (Jenny *et al.*, 2014). They also limit the ability to study a single core at high resolution. Despites these disadvantages, these techniques can quantify the rate of sediment transfer and the relative contribution of source material (e.g. Pulley *et al.*, 2015). Non-destructive methods, such as XRF core-scanning (e.g. Arnaud *et al.*, 2016), or magnetic susceptibility measurements (Borruel-Abadía *et al.*, 2015), do not provide any direct quantifications of sedimentary inputs (Brosinsky *et al.*, 2014a; 2014b). While these non-destructive methods may provide some information on the sedimentary organisation at millimetre or micrometric scale, only one longitudinal profile is analysed, which prevents a 2D representation. Alternatively, a multi-dimensional representation can be achieved through imaging techniques (e.g. photography, radiography), but to date these methods do not provide information on geochemistry or sediment composition and have not been applied in a source-to-sink context (Owens *et al.*, 2016).

In this study, we propose a new experimental method based on hyperspectral imaging. The goal of this research is to track the nature and origin of sediments stored in a lacustrine deposit following a source-to-sink approach. Applied to a sedimentary archive, this imaging technique is effective because it can be carried out at the high-resolution, is non-destructive, multi-dimensional, and can provide quantitative data (Butz *et al.*, 2016; Van Exem *et al.*, 2018). Essentially, numerous bands of reflectance are measured in 2D, and each pixel contains one full reflectance spectrum. This technique can provide information at the micrometer scale, and therefore seasonal and extreme events can be discerned (Dearing *et al.*, 2010).

In order to test this method, we have selected a lacustrine core from the proglacial Lake Linné (Svalbard archipelago, Norway), located along the north-western coast of Spitsbergen. Holocene lacustrine deposits in this lake consist of finely laminated sediments (Mangerud and Svendsen, 1989; Svendsen and Mangerud, 1992; Snyder *et al.*, 2000) with only one major OM (organic matter) layer originating from a coal bed outcrop within the catchment (Svendsen and Mangerud, 1997). The catchment is generally devoid of soils, the vegetation is limited to sparse lichens and moss (Gogolek and Lewandowski, 1980) and no indicator of primary productivity is observed in the sediment of the lake (Svendsen *et al.*, 1989; Svendsen and Mangerud, 1992, 1997; Snyder *et al.*, 2000). Due to the relatively simple nature of organic matter accumulation in the lake, this site is an excellent location to test the hypothesis that the hyperspectral signature (calibrated with other traditional, destructive methods), can accurately reconstruct the Total Organic Carbon (TOC, expressed in weight %). This challenge is relevant since TOC of lacustrine sediment is a proxy widely used in palaeoenvironmental studies in the Arctic context (Bakke *et al.*, 2013).

Within a source-to-sink context, we present two methodological approaches based on hyperspectral imaging. In the first approach (A), we compare the spectral properties of downcore samples with samples collected from the lake catchment. The second approach (B) entails the identification of end-member spectral signatures from within the sediment core itself (without the use of catchment samples). Results from these two approaches are then compared with a particular focus on the unique source of OM (coal). TOC based on the hyperspectral imaging method are then calibrated and validated with the use of a bulk organic geochemical method (Rock-Eval 6 pyrolysis).

2 Study site and materials

2.1 Study site

Lake Linné (Linnévatnet) [78°03'N; 13°50'E] is located at the north-western coast of Spitsbergen in the Svalbard archipelago, Norway, (figure 1A). The lake is 4.6 km long and 1.2 km wide and is divided into three sub-basins with various depths (Mangerud and Svendsen 1989). The northern basin is the largest (75 % of the lake surface area) and has a maximum depth of 30 m. The two southerly sub-basins are less than 15 m deep. The south-western basin is characterised by a delta fed by a stream draining an old glacial cirque (referred as the Little Ice Age (LIA) cirque). The other sub-basin is impacted by water and sediment discharge from the Linnélva River that forms a delta at the SE shore of the lake. Linnélva, sourced mainly from the glacier Linnébreen, drains a catchment of 37 km^2. The maximum elevation within the watershed is Griegfjellet (778 m a.s.l., figure 1B). The watershed is composed of three different rock types which outcrop from east to west, the rocks in the Eastern watershed belong to the Gipshuken Formation dated to the middle Carboniferous; the valley bottom is formed of rocks from the Orustdalen Formation of Lower carboniferous age and the ridge and upland cliffs in the West are a Precambrian bedrock phyllitic rocks of the St. Jonsfjorden group (figure 1A). There is an outlet at the north end of the lake that drains into Isfjorden.

Lake Linné was formed by glacial activity during the pre-Holocene period (Boyum and Kjensmo, 1978; Svendsen *et al.*, 1987). During the Early Holocene, the Linnédalen valley was a fjord inlet, evidenced by marine terraces along the valley walls (Mangerud and Svendsen, 1989). The lake was isolated from the fjord around 9600 BP (years before present) due to isostatic rebound (years before present), (see also Mangerud and Svendsen 1989; Svendsen and Mangerud 1992 for detailed characteristics and history of the lake).

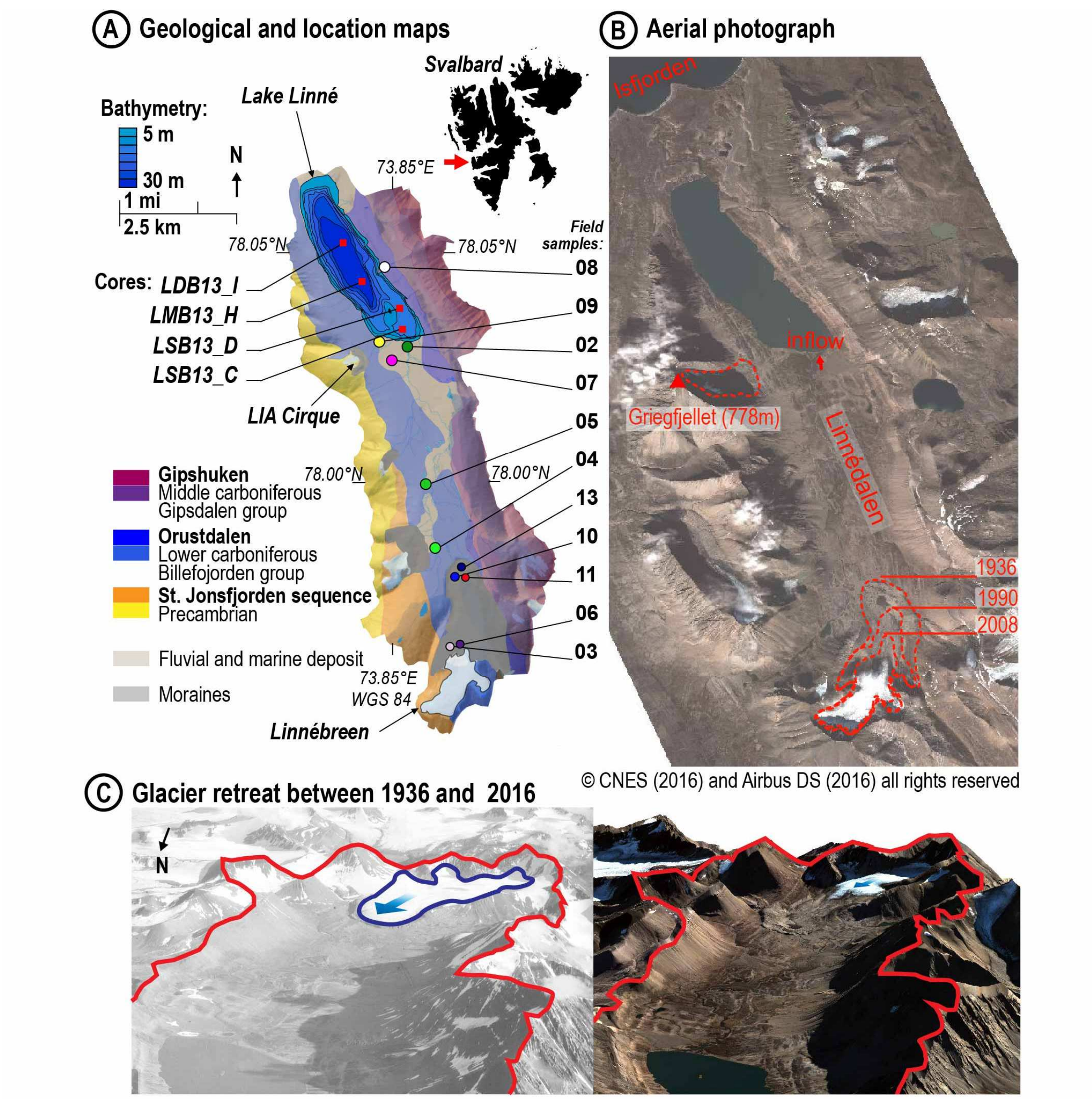

Figure 1 : *A: bathymetric and geological maps of the Lake Linné and its catchment with sampling and coring sites. B: Satellite Pleiade image in July 25th 2016 and the maximum*

expansion of the glacier for the years 1936 (Svendsen and Mangerud, 1992), 1990 (Dallman et al., 1992) and 2008 (Landsat image, Norsk Polar Institute, NPI). C: geographical position and expansion of Linnébreen in 1936 and the DEM (NPI, CNES and Airbus DS, 2016 data). Red line: the catchment limit.

2.2 Expected sedimentary sources

The first and likely dominant sedimentary source for the lake is located in the south part of the catchment where the Linnéelva River delivers sediment from the erosion of the Linnébreen glacier into the lake (Svendsen and Mangerud, 1997). This solid export is highly impacted by local coal beds and by a limited input of limestones (3-6 wt.%, Snyder *et al.*, 2000) from the Orusdalen formation (Billefjorden group, Lower Carboniferous, figure 1A). Orusdalen rocks are composed of sandstones with plant fragments, black marls and coal beds (Dallmann *et al.*, 1992). This source is estimated to be responsible for half of the yearly sediment flux delivered to the lake (Svendsen *et al.*, 1989). The contribution of coal likely exhibits first-order control on the TOC of Lake Linné sediments, as evidenced by the linear relationship observed between TOC and coal concentration (Mangerud and Svendsen, 1989, 1997).

The second important sediment source is located in the eastern part of the catchment, which is drained by an ephemeral stream episodically fed by groundwater and nival melt water. Sediments from this stream are mainly composed of limestones (10 to 40 wt. %) with a minor amount of coal (<1% wt.%) (Snyder *et al.*, 2000). A ferrous and dolomitic gypsum outcrop is present in the eastern part of the valley (Gipshuken deposit from the Gipsladen formation, figure 1A) but its contribution to the sediment flux exported to the lake is thought to be insignificant (Snyder *et al.*, 2000).

The third source, located in the western part of the catchment, consists of low grade metamorphic sediments depleted in limestones (3 to 6 wt.%) and graphitic OM (< 0.2 wt.%) from the LIA cirque installed downstream the Griegfjellet Mount (Snyder *et al.*, 2000). These rocks, corresponding to arenitic phyllites, are of Precambrian to Ordovician age and are considered as the bedrock of the catchment (rocks from the St. Jonsforden sequence, figure 1A). Late Holocene glacier activity in the western part of the watershed, such as within this LIA cirque, is evidenced by the occurrence of some moraines (Reusche *et al.*, 2014).

The last source is the marine sediments deposited prior the isostatic rebound and related to the ice cap retreat in the valley during the last ice age. However, according to Svendsen *et al.* (1989), these sediments remain insignificant with respect to the sedimentary budget of the lake. There are further limited outcrops of marine-derived material and riverine sediment throughout the valley (Dalmann *et al.*, 1992), their influence on sedimentation in the lake is negligible althrough wave washing and soliflucted sediments along the shorelines has been observed during fieldworks. The sediment sources listed here have been identified in the lacustrine sediment record based primarily on comparison with soil and catchment samples collected in the field (see below).

2.3 Provenance samples

All samples collected in the field are listed in table 1 and encompass the main sources previously described in section 2.2. 11 samples were collected at the different rock outcrops: the first source (labelled I) is characterised by moraine samples from the Linnébreen glacier, rock flour sampled on the glacier, and fine sediments stored between the glacier and its moraine (figure 1A, sample number: 03, 06, 10, 11 and 13). The second source (II) is identified by a unique sample coming from the LIA cirque (figure 1A, sample number 09). The third (III) is mostly limestone characteristic of the eastern cliffs formed by the Gipsuken formation (figure 1A, sample number 08). The last source (IV) is defined by the marine terrace sediments sampled in the Linnédalen valley (figure 1A, sample number 07) and by some riverine samples deposited in an intermediate storage area (floodplain area) or in the flood deposits (figure 1A, sample number 02, 04 and 05).

Table 1 : *Field samples and sedimentary core description.*

Sample/core	East/long.	North/lat.	Type	Description
02_LowerLinnélvased	13.8603°	78.02887°	fine sediment	Lake fan of Linnéelva
03_SurGlacierLinnéFront	13.9193°	77.9702°	fine sediment	Glacier front deposit
04_ SkStreamSed	13.88765°	77.98452°	coarse sediment	River deposit
05_ MidLinnélvaSed	13.87832°	77.99922°	fine sediment	River deposit
06_BulkSedFront Glacier	13.9137°	77.9691°	fine sediment	Melt flow stream deposit
07_ MarMudSed	13.84733°	78.02835°	fine sediment	Marine terrace
08_Linnécarbonatefan	13.83692°	78.04625°	coarse sediment	Lake fan of east stream
09_ OldCirque	13.84622 °	78.0295°	fine sediment	Lake fan of LIA cirque stream
10_EDMoraine	13.9116°	77.97717°	bulk « coal »	Morain deposit
11_LinnéGlacierCoalAffl.	13.9239°	77.9771°	bulk rock	Coal rich sandstone
13_CoalGLMor	13.9164°	77.9792°	bulk « coal »	Moraine deposit
LDB13_I	13,8014°	78.0507°	sediment core	37.5-m depth
LMB13_H	13,8156°	78,043°	sediment core	37.5-m depth
LSB13_D	13,8561°	78,0372°	sediment core	14.5-m depth
LSB13_C	13,86611°	78,032°	sediment core	14.5-m depth

2.4 Core description

Four sediment cores were collected from the Lake Linné with a gravity coring system during the 2013 summer expedition (August). Two cores were taken from the northern sub-basin: core LDB13_H (60 cm long, ISBN number: IEM2C0013) was collected towards the delta of a small tributary draining the eastern cliff (figure 1A), while the distal core LDB13_I (70 cm long, ISBN number: IEM2C0014) was taken from the deepest part of the lake (water depth of37.5 m, table 1, figure 1A). Two cores were taken from the SE lacustrine sub-basin, which is fed by the Linnélva delta: LSB13_D (61 cm long, ISBN number: IEM2C0012) was taken close to the main basin while core LSB13_C (52 cm long, ISBN number: IEM2C000Z) was sampled just in front of the mouth of the Linnéelva delta (figure 1A). Methods

2.5 Hyperspectral imaging

2.5.1 Method description

Hyperspectral imagery is a visible and near infra-red spectroscopic method measuring the reflectance of sediment surface exposed to an incident light. Light absorption by the sediment results in a reflected light which mainly depends on the composition. Hyperspectral core-logging consist in acquiring an image of a whole sediment core in a single scan. The measure, expressed in percentage of reflectance after a radiometric calibration (3.1.3 Reflectance normalization), is provided for each pixel of the image. The data treatment consists to infer the sediment composition by analyzing the reflectance spectra. Hence the results are represented depending on the position of the pixels to describe the geochemical variations at high resolution.

2.5.2 Raw data acquisition

Prior to analysis with the hyperspectral camera, field samples were crushed in agate mortar after being dried in a ventilated oven at 30°C. The sediment cores were split and cleaned/scraped to ensure a uniform sediment surface. The acquisition process was performed on a core logger equipped with a hyperspectral camera (VNIR-PFD, SPECIM®). This technique has both a short sampling time and allows for high spatial resolution (several dozens of µm). The distance between the studied sample / core and the camera lens was 130 mm, with an acquisition angle of 0°. The surface of the sample is indirectly illuminated by 18 halogen bulbs homogeneously distributed around the lens. The acquisition speed of the core logger was 0.5 $mm.s^{-1}$. Pixels from the final image exhibit a spatial resolution of 47x47 $µm^2$ and contain raw spectral data from 400 to 1000 nm at 6.5 nm spectral resolution (given in digit number, DN).

2.5.3 Reflectance normalization

For each acquisition, a normalisation process was performed, with a standard material panel (SPECTRALON®) that exhibited 99 % reflectance. This was then used to convert raw data (8 bits) into reflectance percentage (figure 2A, B). All of the measurements were normalised based on this 99% reflectance value. Data processing was then carried out with the ENVI software (v. 5.3). Once normalised, the measurements bands from 475 to 1000 nm were selected in order to keep a signal-to-noise higher than 2. Signal processing included several steps: preprocessing was used to clean up the data, then a first spectral library was made up based on the extraction of the end-members from the sediment core hyperspectral image and a second library was made up of the field samples reflectance measurements. Data processing consisted of the correlation of the sediment core spectra with the libraries separately to form two classification images.

2.5.4 Image preprocessing of downcore sediment

It is crucial to preprocess the image of the sediment core to identify and delete outliers (figure 2A, B). Changes in surface roughness can form shadow zones and produce reflection of water present either in sediment cavities and/or on mineral or grain faces. To avoid misleading interpretations, pixels that exhibited grey scale values that exceeded an empiric threshold of 1.5 times the standard-deviation of an image were removed; in this study, such pixels corresponded to ~5 % of the total archive.

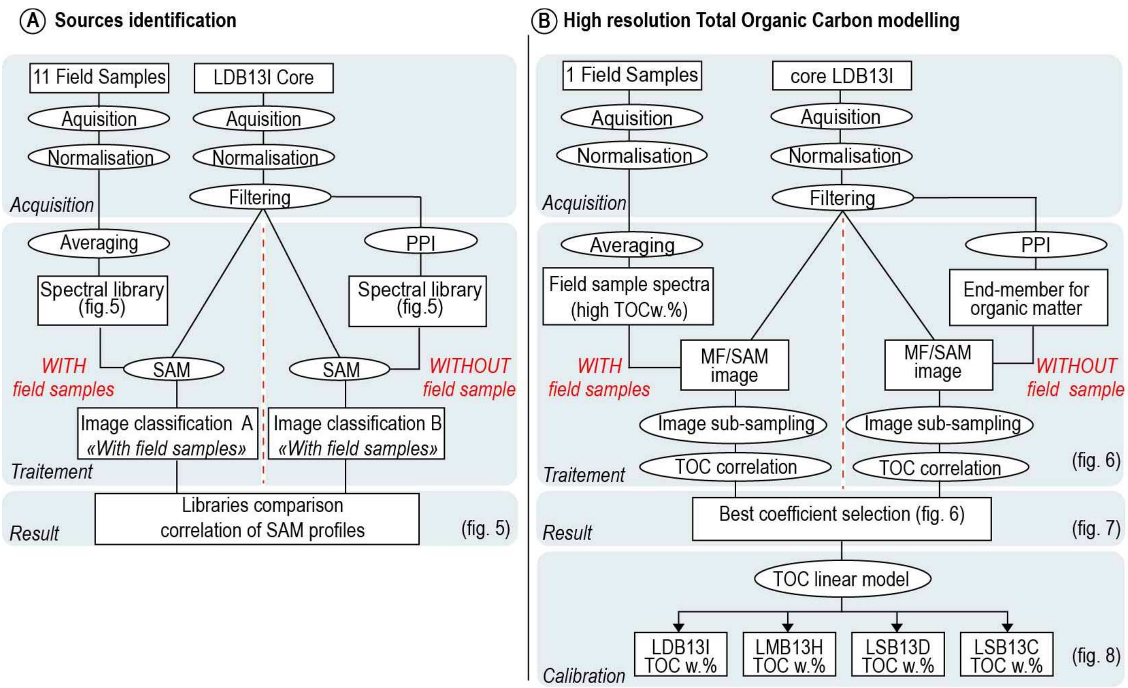

Figure 2: *A: Hyperspectral method used to discriminate the sedimentary sources and protocol steps following a common approach and a new approach using end-members of the spectral library. B: Quantification of the signal from the total organic carbon content (TOC, in wt.%), Comparison of the two approaches and TOC reconstruction on the sedimentary archives (see section XX for further details).*

2.5.5 Library A: including provenance samples

For the Library A approach, the hyperspectral library (against which downcore samples are compared) consists of spectral references from samples collected within the catchment of Lake Linné (figure 1), with the objective to characterise the main sources of the sediments preserved in the lake. The 11 field samples were positioned in a glass petri dish with a minimum thickness of 5 mm and measured in a single run. The image was divided into square areas of at least 500 pixels each. The area was averaged to provide one spectral reference by field sample. One specific color is assigned to the reference spectra.

2.5.6 Library B: excluding provenance samples

Library B excludes any field samples collected from the Linné catchment and instead relies on spectral “end-members” extracted directly from a previously measured sedimentary archive (Butz *et al.*, 2015). This step is performed using "ENVI spectral wizard", in which a MNF filter ("Minimum Noise Fraction", Green *et al.*, 1988) is applied. The end-members are selected according to the pixel purity index (Pixel Purity Index, PPI). This algorithm selects the most highly differentiated spectral signatures of a given hyperspectral image (Boardman, 1994) and thus, of the sedimentary archive.

2.5.7 Classification by spectral angle

Spectral Angle Measure (SAM) is used to classify spectra of an image from the spectra of a hyperspectral library (Kruse *et al.*, 1993). SAM returns a value between 0 and 1, with values closer to 0 representing closer spectra. The classification assigns the same color of the closest library spectra to the pixels of the sediment core image. Finally, the classification image indicates which is the closest field sample (or end-member) to the different parts of the sediment core.

2.5.8 Hyperspectral imaging calibration by Rock-Eval 6 pyrolysis

To convert the imaging data into total organic carbon (TOC), a calibration curve was established that relate measured TOC (wt.%) through Rock-Eval 6 pyrolysis and the MF / SAM hyperspectral index (similarity assessment by Match Filtering, MF, divided by the spectral angle, figure 2B). In order to amplify the degree of variation between spectra, the convolution product (i.e. Match Filtering) was divided by the spectral angle (Crassard *et al.*, 2013). A spectrum related to OM content was used to calculate the MF / SAM index of the archive. The image of the MF / SAM index was sub-sampled into 71 zones corresponding to the samples analysed by Rock-Eval 6 pyrolysis (1x1 cm², see below). A transfer function was then defined using these 71 values. To plot the TOC over the sediment core image from the "with field samples" library, the reference spectrum of the sample with the highest TOC was selected. For the end-member library, the OM spectrum was selected based on low reflectance and monotonous spectrum (Cloutis *et al.,* 1990). These properties are specific of geological coal spectra (Cloutis, 2003) and to a mixture of mature organic matter and clay (Milliken and Mustard, 2007).

2.6 OM study with Rock-Eval 6 pyrolysis

Rock-Eval 6 pyrolysis (Vinci-technology®) was used to measure and calibrate TOC from the Lake Linné sediment core. This method relies on thermal degradation of OM at gradually increasing temperatures through pyrolysis and combustion. Pyrolysis provides the TOC of a given sample along with other geochemical characteristics related to the origin and alteration states of the OM (Lafargue *et al.*, 1998). Originally developed to describe the oil potential of sedimentary rocks, the method is widely used to characterize recent OM in soil (e.g., Disnar *et al.*, 2003), lacustrine sediments (e.g,., Di-Giovanni *et al.*, 1998; Disnar *et al.*, 2003), and suspended sediments in rivers to track fossil organic carbon (Copard *et al.*, 2006). Contrary to other methods related to TOC quantification, the main advantage of this technique is that it does not require pretreatment (acid digestion) since the thermal decomposition of carbonates is considered (see Lafargue *et al.*, 1998 for the principle of the method). Based on standard analyses, the uncertainty of the reconstructed TOC is 0.03 wt.% (Noel, 2001). Analyses were performed on 71 samples from LDB13_I core (1 cm^3), sampled each centimeter, and on 11 field samples. The field samples were crushed at 250 µm and dried in a ventilated oven at 25°C. 50 to 80 mg of sediment was analyzed per sample. For the first stage of the pyrolysis, samples were heated in oven beginning at 200° C. The temperature was then increased to

650°C at a rate of 25°C min^{-1}. During this process the pyrolysis effluents are conveyed with a constant nitrogen flow to the flame ionization detector for the quantification of hydrocarbons and to an infrared detector for the quantification of the CO_2 and CO compounds. The second oxidation phase was carried out in an oven where the carbonaceous residues of the pyrolysis were carbonized between 400°C and 750°C and the effluents exported via airflow to an infrared detector where CO_2 and CO were quantified. These signals give some parameters related to the quantification of TOC and the quality of the OM: TOC (in wt.%) is given by the sum of OC pyrolyzed (pyrolyzed carbon) and carbonized OC (residual carbon), while the pyrolysis step gives qualitative parameters of the OM. In this study, we focused on the richness of hydrocarbons of the OM (HI index, expressed in mg $HC.g^{-1}$ TOC) and that of the oxygen (OI index, expressed in $mgO_2.g^{-1}$ TOC).

3 Results and interpretations

3.1 Stratigraphy and sedimentary units

Core LDB13_I was divided into 3 units (1-3) based on the dominant color and thickness of the laminations (figure 3). Unit 1 (0-7 cm depth) of the LDB13_I core is dark grey and was divided into three subunits based on lamina thickness. The subunits 1A and 1B of 0 to 3 cm deep both highlight lamina of heterogeneous thicknesses of about 1-mm with clear or even gradual contacts. In the distal core LDB13_I these 2 subunits are not distinguished from each other. In the proximal records (i.e. LSB13_C and LSB13_D), the color of the laminae is clearer in the 1A subunit. Subunit 1C (3 to 7 cm deep), has laminations less than 1-mm thick and sharp contacts (figure 3). Some bright yellow laminae are present. Unit 2, from 7 to 34 cm, shows alternating light and dark laminae. Subunit 2A, 7 to 10 cm, is bright, the thickness of the lamina varies from 1 to 3 mm. Contacts are sharp or gradual. Subunit 2B 10 to 16 cm deep is dark, the thickness of the lamina is homogeneous and approximately 1 mm. The contacts between the lamina are clear. Subunit 2C (16 to 34 cm depth) is clearly defined. The laminae thickness is heterogeneous from 1 to 3 mm. The contacts are sharp. At 25 cm depth in Unit C, a red lamina (2 mm) strongly emerges from the rest of the entire archive. This lamina is also present at 35 cm in the LDB13_H archive. Unit 3, 34 to 71 cm, is heterogeneous with fewer laminations than the previous two units. In the LDB13_H archive, the sediments of Unit 3 have a massive appearance (figure 3).

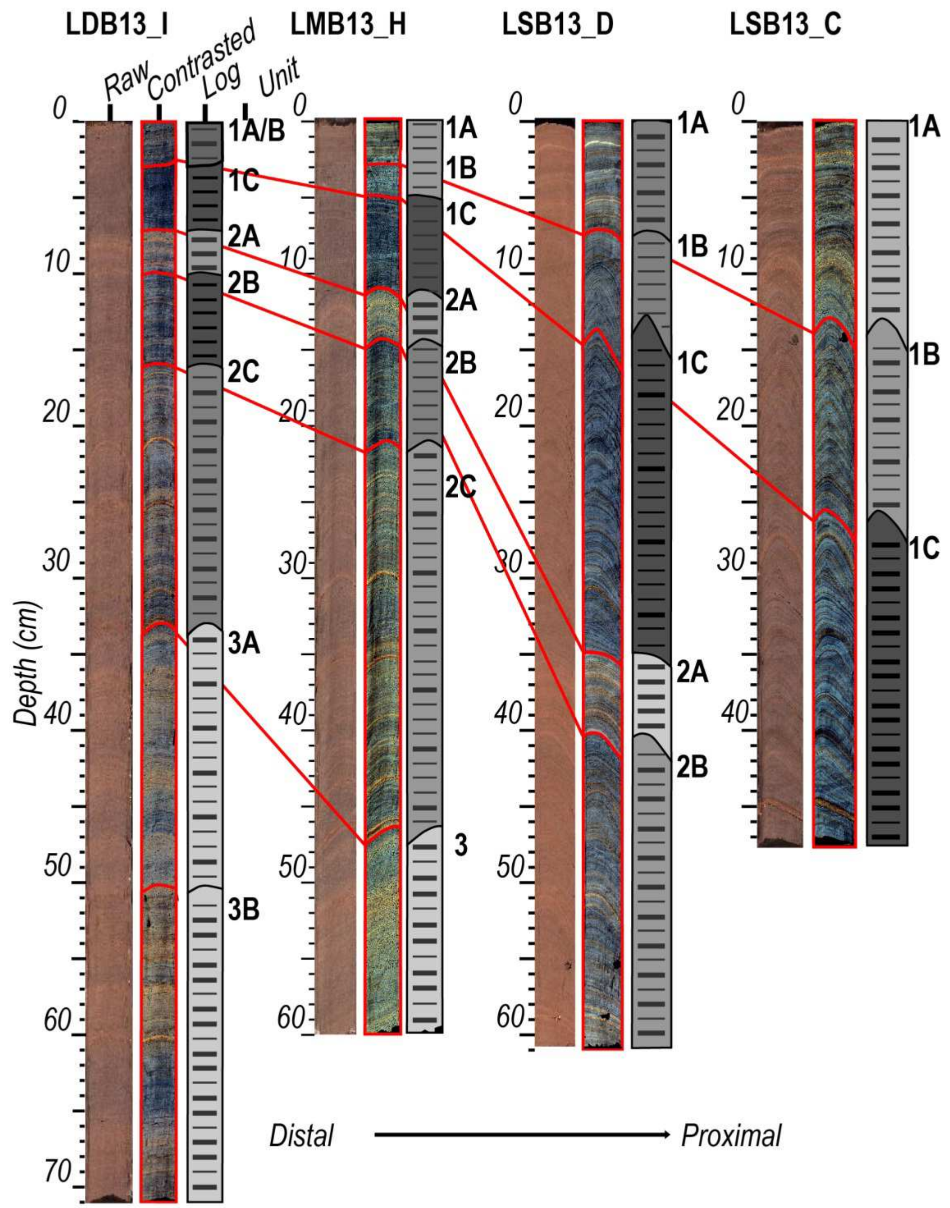

Figure 3: *Raw hyperspectral images and hyperspectral images with amplified contrast, sedimentary log, and correlation of sedimentary units between the four archives.*

Although the subunit thickness appears to increase from LDB13_I core to LSB13_C core, the same stratigraphy is exhibited in all four archives. This difference in thickness is explained by the locations of the coring sites. The distal cores (I and H) receive relatively less sediment because they are located further away from the Linnéelva than the proximal sites (C and D). The sedimentary deposits of the LDB13_I core are representative of the stratigraphy of the other cores and the archive can therefore be used to describe the sedimentary inputs in the Lake Linné. The following interpretations are based primarily on the LDB13_I archive since it presents the thinner laminations to experience the high resolution of the hyperspectral core-logger.

3.2 OM geochemical analyses

The total organic carbon (TOC) in the LDB13_I core varies from 1.58 to 3.41 wt.%, with significant variability with depth (figure 4). The highest values are found in sub-units 1C and 3B (> 3 wt.%). The TOC for the field samples range from 0.3 to 6.74 wt.%, where the highest values (i.e. > 5 wt.%) correspond to the Linnébreen moraine coal-rich samples (i.e. 10 and 13). Fluvial sediment samples have intermediate values (0,58 to 2,47 wt.%). The Sample 04_SkStreamSed located upstream the Linnéelva has the lowest TOC content of the fluvial source (0.58 wt.%). This reflects a low influence of the glacier sediment at the sample location, slightly on the west of the glacier (figure 1). All other samples show low TOC (< 1 wt; %, figure 4A), indicating a gradual dilution of OM inputs from the Linnébreen glacier by lateral contributions. However, these lateral contributions remain low since the TOC are 2.17 wt.% at the mouth of the stream (02_LowerLinnéelva). Samples from the three other potential sources (sample 09_OldCircle, 08_LinnéCarbonateFan, 07_MarMudSed) also exhibit low TOC: 0.03 wt.%, 0.19 wt.%, 0.75 wt.% respectively. It should be noted that the top core sample exhibits a TOC ~2.50 wt.%, similar to samples along the stream (at the intermediate site: 05_MidLinnéElvaSed: 2.47 wt.%, slightly upstream of the Linnéelva River mouth: 02_LowerLinnéElvaSed: 2.17 wt.%).

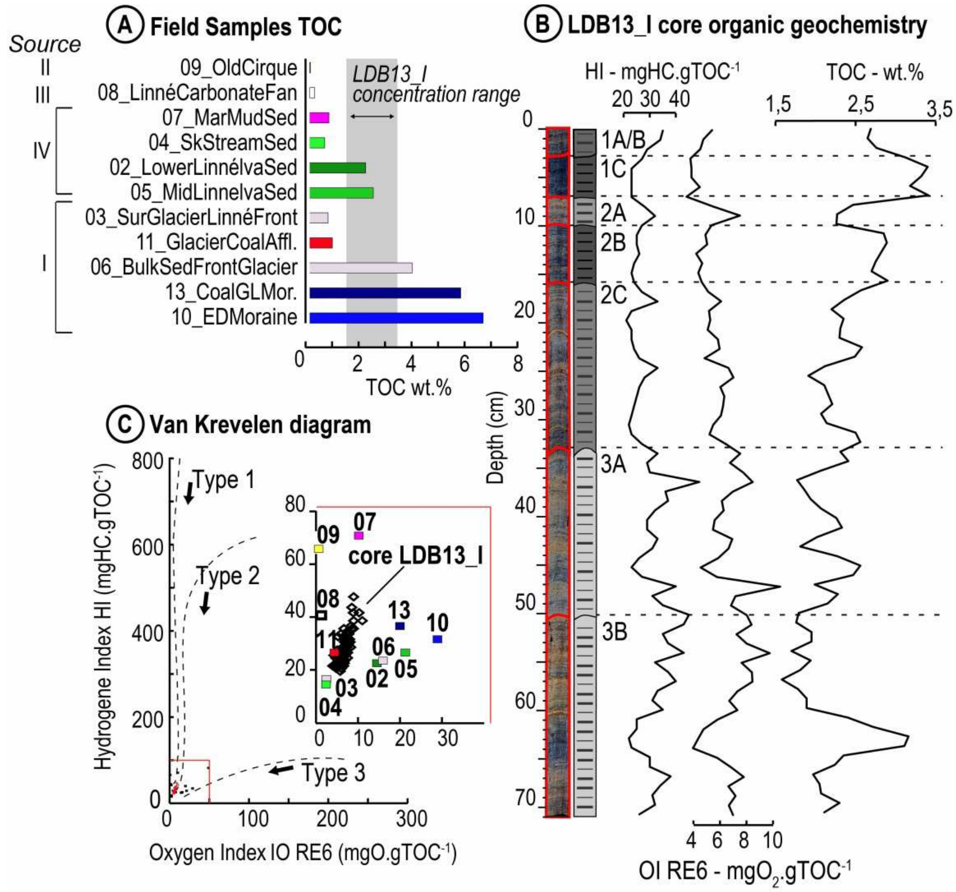

Figure 4: A: Total Organic Carbon (TOC% m) measurements for sediment field samples. B: Hydrogen index, oxygen index and TOC profiles for the LDSB13_I archive. C: Van Krevelen diagram showing oxygen index versus hydrogen index, for field samples and samples from archive LDB13_I. Organic matter (OM) of Type 1 corresponds to kerogens of lacustrine origin, OM of Type 2 corresponds to kerogens of marine origin, OM of Type 3 are kerogens of lignocellulosic material with a terrestrial origin.

OM origin was determined by plotting the OI vs HI index in a pseudo Van Krevelen diagram (figure 4C). For all field samples, OI values are less than 30 mg O_2.TOC^{-1}. HI values are below 70 mgHC.TOC^{-1}. This range of values suggests that the OM of the Linnéelva watershed has a lignocellulosic origin and is likely related to glacier erosion of the Carboniferous coal seams. Samples from other parts of the watershed have a stronger HI (09_Oldcirque, 08_LinnécarbonateFan, 07_MarMudSed: 67, 42, 72 mgHC.TOC^{-1} respectively) and / or very low OI values (09_Oldcirque: 0.12 O_2.TOC^{-1}, 08_LinnécarbonateFan: 9.98 mg O_2.TOC^{-1}).

In the LDB13_I core, the variations of the OI and HI indices are minor with 4 to 10 mgO_2.TOC^{-1} and 20 to 50 mgHC.TOC^{-1} respectively. Compared to the field samples, intermediate values from downcore samples confirm that the sediment deposited in the lake represents a mixture of coal (high OI, low OI) and another source that increases the HI and decreases the OI values. This relationship is particularly evident when comparing HI, OI and TOC values: TOC values are higher when OI and HI values are lower (figure 4B). This clearly contrasts the coal from Linnéelva and detrital sedimentation, devoid of OM, from other sources. However, the RE6 pyrolysis does not provide information on the source of additional OM beyond coals. Essentially, only the remobilization of the geological OM contained in the Carboniferous sedimentary rocks explains the geochemical signature of the OM in the core (figure 4). The OM of core LDB13_I is identical to that identified in the field samples (figure 4A, 35C). The HI and OI values remain broadly unchanged with depth, suggesting an absence of diagenetic processes in the core (figure 4C). One of the main conclusions drawn from the downcore bulk geochemical data is that there is limited autochthonous primary productivity occurring within the lake itself, or at least that this OM is no more present in the lacustrine sedimentary record at the time of the analyses.

3.3 Sedimentary sources tracking with hyperspectral imaging

3.3.1 Approach A: “with field sample”

The spectral library from the field samples, used to identify the sources of sediment material in the core, is presented in figure 5A. These spectra have well-differentiated characteristics in terms of amplitude and slope; as an example, the amplitudes vary from 3 to 19% R (reflectance). The weakest reflectance corresponds to the samples from source I (Linnébreen moraine). The spectrum of the LIA cirque sample (09_OldCirque) differs from the others by increasing sharply between 500 and 600 nm and decreasing between 800 and 900 nm. This significant increase between 500 and 600 nm is related to the occurrence of hematite with the charge transfer of Fe cations within the sample (Hunt, 1977, Deaton and Balsam, 1991, Clark *et al.*, 2007). This is consistent with field observations made during sample collection where yellow oxidized sediment was observed near the sample location. Spectra from the other darker samples exhibit rather lower reflectance values. The spectrum of the sample from the carbonate cliffs increases almost linearly over the entire spectral range to reach 19%R at 1000 nm (08_LinnéCarbonateFan). The spectra of the coal samples from the Linnébreen glacier moraine exhibit reflectance values of less than 5%R (i.e. 13_CoalGLMoraine, 10EDMoraine) with a similar trend. Fluvial sediment samples show intermediate values consistent with a dilution signal (7-14%R for 05_MidLinnéElvaSed sample, 6-12%R for 02_LowerLinnéElvaSed, 5-9%R for 04_SkStreamSed). Finally, the spectrum from the marine terrace sample exhibits intermediate reflectance values ranging from 5 to 11% R (07_MarMudSed).

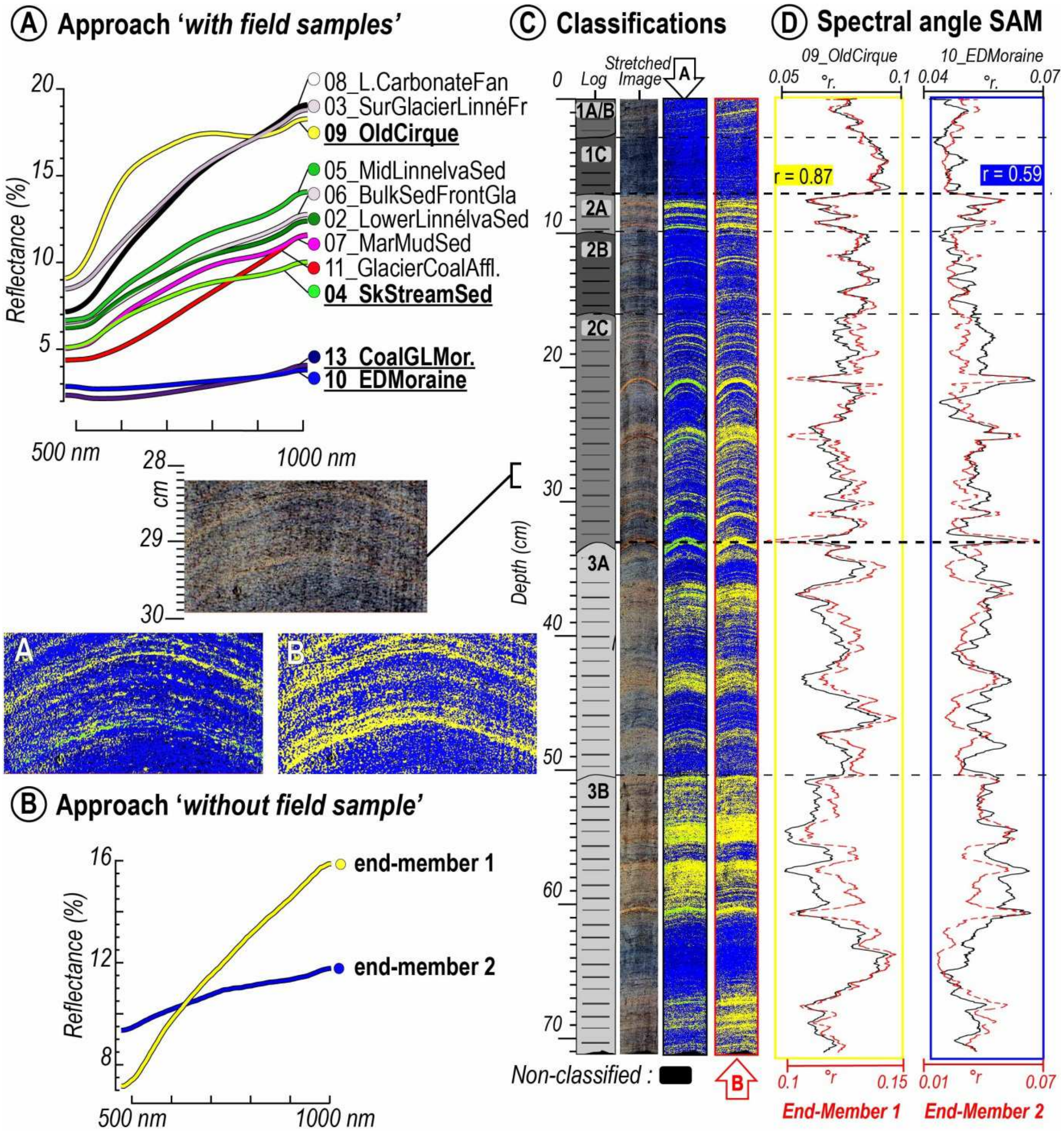

Figure 5: *Results of the identification of the sources. A: hyperspectral library of the approach with field samples, the reference spectra present in the classification are indicated in bold. B: Hyperspectral library of the approach without sample. C: Classification of the LDB13_I archive according to the most similar reference spectra. D: Spectral angle between the reference spectra and the sedimentary archive (average over the width of the image (622-pixels), the average is affected by the curvature of the lamina related to the piston, and moving average on 100-pixels (~ 5.7-mm) in depth).*

Downcore sediment samples were then classified based on these catchment reference spectra using the SAM method. Of the measured catchment samples, four spectral signatures appear to dominate the downcore spectral analyses (figure 5C). The 10_EDMoraine and 13_CoalGLMor signatures are the most prevalent throughout the core (figure 5C). These samples were taken a few meters away from each other and exhibit comparable spectra and reflectance distribution, with the 10_EDMoraine spectrum the most represented. A third spectrum corresponds to the 09_OldCirque sample, taken downstream of the LIA cirque. Downcore spectral signatures that correspond to this reference sample likely represent sediment sourced from this cirque. The last spectrum is the least represented and related to the fluvial sediment sample (04_SkStreamSed). The thick laminae of unit 2C are all attributed to this field sample. Individual laminae that may be difficult to identify visually are clearly distinguished using this hyperspectral method. These submillimeter size laminae, observed all along the core, correspond to changes in the origin of the sedimentary inputs to the lake (figure 5). Among the four sources present in the watershed, three are identified in the sediment core (figure 5C). Neither the source of the marine sediments were evidenced in the archive (sample 07_MarMudSed); nor that of the carbonate cliffs (sample 08_CarbonateFan).

Changes in sedimentary input from the two main sources are characterized by the profiles of their spectral angles (SAM index, samples 10_EDMoraine and 09_OldCirque, figure 5D). Regardless of the number of spectra composing the spectral library, the classification does not attribute all the pixels to a reference spectrum (i.e. "unclassified" zones, figure 5C). Thus, if a source has not been sampled, the core sediment will not be assigned by any similarity with the classification.

3.3.2 *Approach B: "without field samples"*

The objective of this second approach is to directly extract spectral end-members from the sample image (PPI) which are then used as reference spectral library. 5000 iterations of the

PPI algorithm made it possible to extract the most different spectra from the archive, which was then compiled to constitute the library of the "no field sample" approach. Values from the first end-member (EM1), ranged from 6 to 16% R, and generally increased strongly between 500 and 600 nm, indicating the presence of hematite (Deaton and Balsam, 1991, Clark *et al.*, 2007). Values from the second end-member (EM2) vary only from 9.5 to 11% R, with less variation than EM1 (figure 5B), characteristic of a spectra from mature OM (Cloutis *et al.,* 1990; Cloutis, 2003; Milliken and Mustard, 2007).

In this classification, EM2 is the most represented, but laminae assigned to EM1 are present throughout the archive. Thick laminae of unit 2C are assigned to EM2 but generally the EM2 laminae are very fine and thus suggest that slight changes in the origin of sediment are tracked by the technique. The SAM index of end-members shows rapid variations and strong amplitudes for these laminae. The variations in the spectral angle correspond exactly to the boundary between two laminae (e.g. 22 cm deep, figure 5C). Broadly this classification method suggests there are two dominant end-members in the sedimentary record and therefore record two main sedimentary sources.

4 Discussion

4.1 Coupling between the two approaches « no samples» vs « field samples »

The EM1 reflectance spectrum shows an increasing signature which becomes amplified between 500 and 600 nm. This trend is typical of sample spectra from the western LIA cirque (i.e., sample 09_Old_Cirque) and of fluvial sediments from the river (02_LowerLinnéElva, 05_MidLinnéElva, 04_SkStreamSed). This increase between 500 and 600 nm is characteristic of the occurrence of hematite (Clark *et al.,* 2007) reported by Hjelle *et al.,* (1986) and Dallman *et al.,* (1992) in the Precambrian, bedrock on the western side of the lake. The EM1 is therefore attributed to inputs from the southwestern LIA cirque since it originates from the

Precambrian bedrock in the western part of the catchment. Indeed, based on these classifications, the laminae corresponding to EM1 with the approach B ("without field samples") are assigned to samples 09_OldCirque and 04_SkStreamSed with the approach A ("with field samples"). These results is in accordance with the TOC measures since these two samples contain little OM (0.03 and 0.58 wt.%), which show the weak influence of the Linnébreen source. Contrary to other sample of the fluvial sample (02_LowerLinnéElva, 05_MidLinnéElva) 04_SkStreamSed, and 09_OldCirque are representative of the LIA glacier sediments.

The EM2 spectrum is characterized by low reflectance and is most similar to spectra from field samples 10_EDMoraine and 13_CoalGLMor. This signature is consistent with TOC values of EDMoraine (6.74 wt.%) and 13CoalGLMor (5.87 wt.%). These relatively high TOC values come from the erosion of the Carboniferous sedimentary rocks enriched in OM that underlies Linnébreen glacier (Svendsen and Mangerud, 1997). EM2 is therefore ascribed to high OM input from the erosional activity of the Linnébreen glacier on the coal-bearing bedrock below. As a consequence and for the classification, the laminae corresponding to the EM2 (approach B: "without a field sample") are assigned to the samples 10_EDMoraine and 13_CoalGLMor (approach A: "with field samples").

The "with field samples" classification also identifies a third source represented by the 04_SkStreamSed fluvial sediment sample that is absent in the "without field samples" approach. However, in the classification of end-members ("without field samples"), the laminae of the sedimentary inputs of fluvial sediments are all attributed to EM2 (figure 5). River sediments were collected in the intermediate storage area, which receives erosion products from the main primary sources (Linnébreen glacier and lateral input of St. Jonsfjorden rock, figure 1A) during spring floods /nival melt. Thus the spectrum of the sample 04_StreamSed represents a mixture between the spectra of the samples rich in OM from the glacier (i.e. 10_EDMoraine and 13_CoalGLMor) and the contributions of the St. Jonsfjorden rocks present in the LIA cirque (i.e. 09_OldCirque). The reflectance and TOC value of the 04_StreamSed sample are intermediate (5 to 9% R; 0.58 wt.%) relative to the primary source samples (e.g., 10_EDMoraine and 09_OldCirque), however the end-member extraction method relies on highly differentiated spectra (PPI; Kruse, 1993). Thus the spectrum of a secondary source is not an extreme signature and is not necessarily identified as a sedimentary source. The method of spectra extraction explains the absence of this third source in the library of end-members. The reproductibility of the method is thus limited mainly to spectrally distinct sources. Hence, if a source exhibits an intermediate spectrum to those of two other sedimentary sources, this source may not be distinguished and is likely to be attributed to one of the other sources of the classification.

The classification assigns a colour code to a specific pixel based on its similarity to the closest spectrum in the library. However, if there is a mixed spectral signal, minor contributions from another source are not considered, similar to the situation for secondary sources in the previous section. It is therefore necessary to use the spectral angle (see 3.1.6) to resolve mixtures of sedimentary sources. Indeed, variations in spectral angle (SAM index, figure 5D) highlight differences in sedimentary input even when the overall spectral signature is not necessarily definitive. The SAM indices of sample 09_OldCirque and sample 10_EDMoraine vary in opposite directions (e.g. they are anti-correlated). Within the classification, this corresponds to variations in the intensity of sedimentary inputs from the Linnébreen glacier and the LIA cirque. The SAM index profile for sample 09_OldCirque increases at the level of the laminae attributed to the 04_StreamSed sample (unit 2C). This confirms that 04_StreamSed is the result of a mixture of sedimentary materials from the Carboniferous formation and the Precambrian Massif.

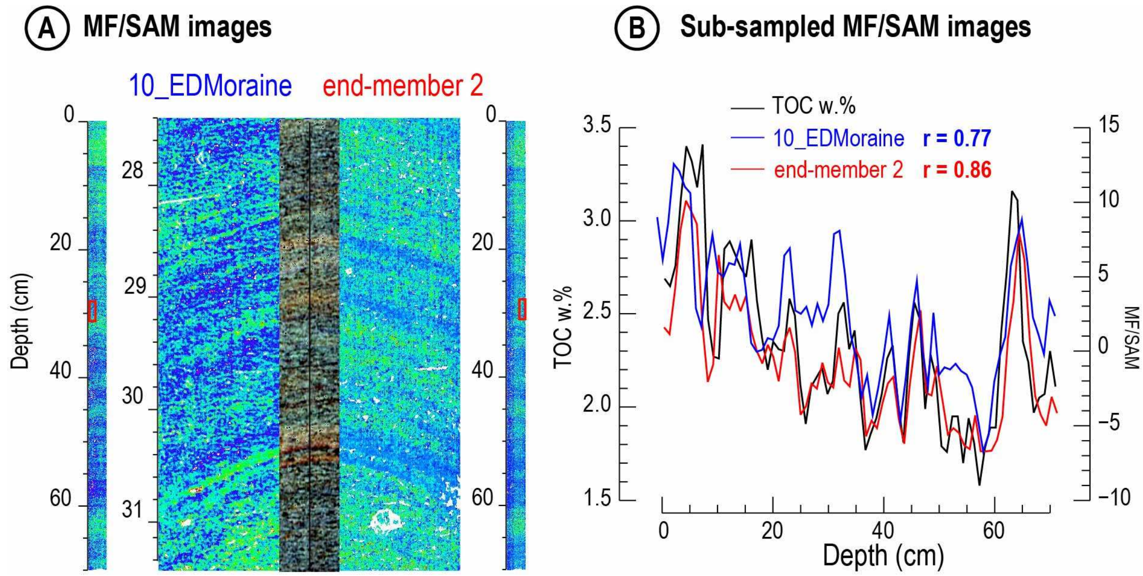

Figure 6: *A: Comparison of images of the MF / SAM ratio of the LDB13_I archive obtained from the spectra of the 10_EDMoraine field sample and the end-member 2 spectrum. B: Correlation between the total organic carbon concentration (% m) of the LDB13_I archive and the MF / SAM ratios of the 10_EDMoraine reference spectrum "approach with field sample" and the end-member 2 "approach without field sample".*

The MF / SAM index of EM 2 characterizes the deposits in greater detail (figure 6). The MF / SAM image of EM2 identifies finer-scale changes in TOC content than the index from the spectrum of the field sample 10_EDMoraine. The 10_EDMoraine sample exhibits a correlation coefficient with TOC of 0.77 while that of the EM2 reaches 0.86 (figure 6B). This difference is explained by the high TOC value of the 10_EDMoraine sample (6.74 wt.%) compared to the sedimentary archive, where TOC values ranged from 1.58 to 3.41 wt.% (figure 4). Additionally, since the EM2 spectrum has been extracted from the LDB13_I core, it is therefore more representative of this range of values. The reflectance values of the EM2 spectrum (i.e. 5 to 9% R) suggest a lower concentration of fossil OM compared to the sample 10_EDMoraine (3% R for 6.74 wt.%; Milliken and Mustard, 2007). Consequently, the MF / SAM index of EM 2 was therefore selected to calibrate the TOC values at high-resolution.

4.2 Sources tracking at high resolution

Three types of sedimentary deposits are identified in the classification, representing contributions of three of the four potential sources defined by Snyder *et al.*, (2000). The first sedimentary source was well characterized and assigned to the coal-bearing Carboniferous rocks that underlie the Linnébreen glacier (Snyder *et al.*, 2000). Svendsen and Mangerud (1997) demonstrated that TOC values in the Lake Linné sediment are correlated with the input of this coal-rich material. Erosion of the Carboniferous rocks enriched in coal by the glacier can be considered as a marker of glacial activity. The predominance of the glacier inputs in the classification is consistent with some previous studies (Svendsen *et al.*, 1989, Svendsen and Mangerud, 1992, 1997, Snyder *et al.*, 2000). Svensdsen *et al.*, (1989) estimated that the volume contribution of glacial erosion to the lake sediments reached 50 %, thus explaining the importance of sedimentary inputs from the glacier.

The second source of material is suggested to be sediments from LIA cirque in the southwestern part of the catchment. Local wind patterns cause currents in the lake to follow a counterclockwise rotation (Snyder *et al.*, 2000). The contributions of the LIA cirque to the west of the watershed are thus diverted towards the east before moving north over the LDB13_I sampling site. Additionally, the input of material by hyperpycnal flow is blocked by the bedrock threshold located between the two sub-basins in the southern part of the lake (Snyder *et al.*, 2000). As a result, it is likely that the input of material from the LIA cirque that eventually ends up at Site I mainly consists of fine material.

Fluvial sediment inputs (sample 04_StreamSed) from the fourth source are identified in this study by the field-sampling approach (04_SkStreamSed, figure 5C). Although the contribution of fluvial erosion has not been documented in previous studies (Snyder *et al.*, 2000), these conclusions coincide with observations made during the field survey. This fluvial source was also reported from Svendsen *et al.,* (1989) who mentioned minor fluvial erosion of Linnéelva channels.

As seen in the previous works of Svendsen *et al.*, (1989) and Snyder *et al.,* (2000), the contributions from marine sediments (i.e., fourth source) and carbonate cliffs were not detected and are thus considered insignificant.

4.3 TOC signal reconstruction at high resolution

We tested the ability of hyperspectral imaging to reconstruct OM concentration in lake sediments by calculating the correlation between TOC and the MF / SAM ratio corresponding to sedimentary inputs from the Linnébreen glacier identified by EM2. In order to more accurately compare the Rock-Eval measurements with the hyperspectral data, the data were re-sampled to match the sampling interval of the Rock-Eval data (figure 7). It is important to note that minor coring effects, visible by the curvature of the lamina (in figures 3 and 5), induces an error in the correlation between TOC measured by Rock-Eval pyrolysis (TOC RE) and TOC reconstructed from hyperspectral imagery (TOC HYP). Between 0 and 5 cm both measured and reconstructed TOC are better correlated. As compression due to coring affects the laminations on the thickness of the core, the effect of coring is amplified by the volumetric measurement of the concentration of TOC RE (volumetric sampling) compared to the hyperspectral analysis, which is based on the measurement of a surface (figure 6). Despite this issue, the correlation between the high-resolution reconstruction of TOC HYP and TOC RE is highly promising. The results confirm the potential of hyperspectral imaging to quantify TOC as the reconstructed TOC values are highly correlated with the measured proxy data ($r = 0.86$) (Figure 6). Based on this relationship, it is possible to reconstruct TOC at high resolution from the other cores collected in Linné that were not analyzed by Rock Eval Pyrolysis.

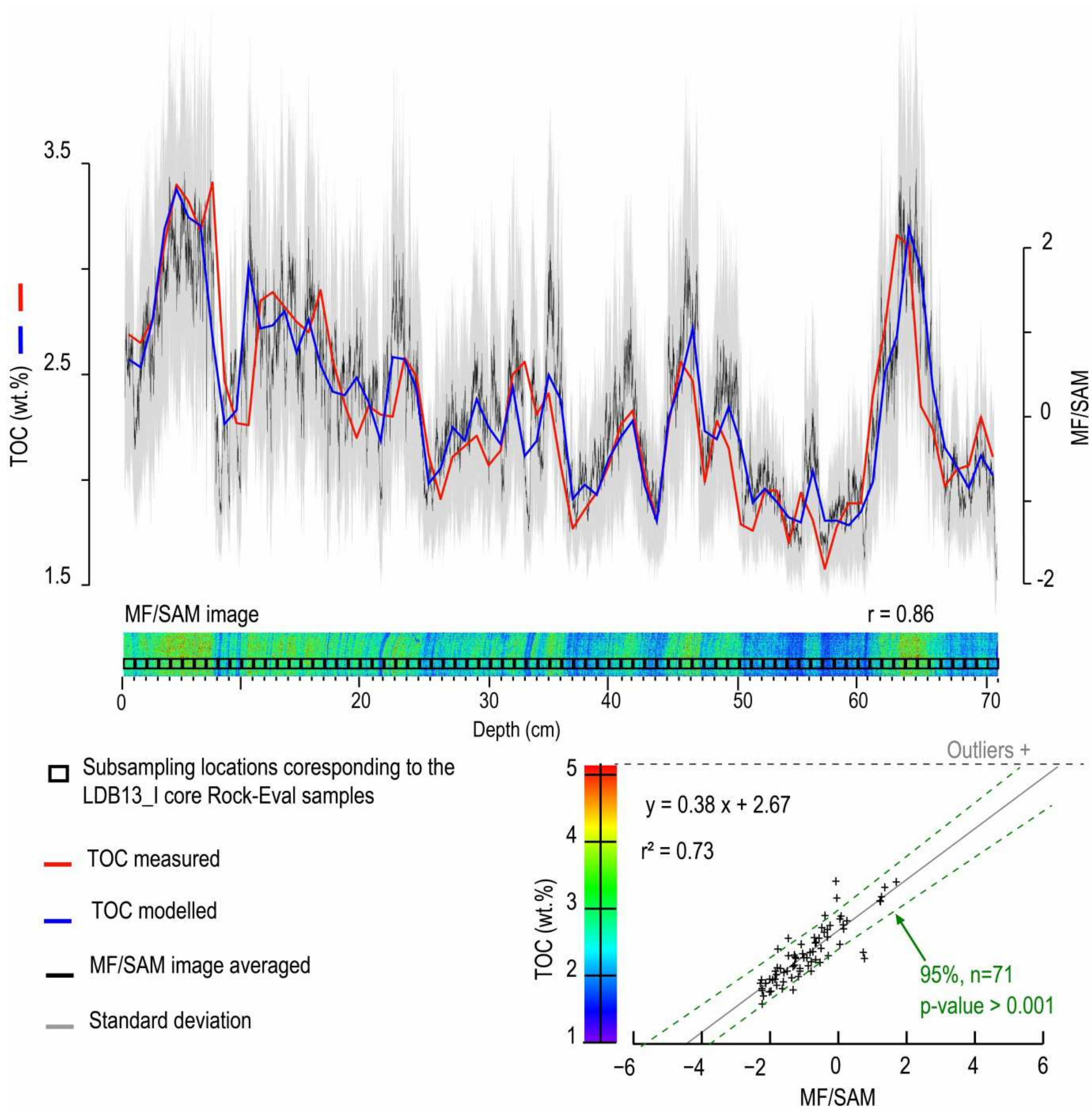

Figure 7: *Calibration of the hyperspectral index MF / SAM by the concentration of TOC (%m) measured by the destructive technique at low resolution. The image is downsampled to establish a transfer function to reproduce the high resolution TOC concentration.*

One caveat to this approach is the necessity of similar sedimentary matrices between the different sediment cores. The correlation between the hyperspectral data and measured TOC concentrations was established based on the reflectance of the organic matter and the Lake Linné specific mineral matrix. This relationship would be different for a different mineral matrix. Additional sedimentary sources, or other types of sediment, could further complicate this correlation. It is unlikely that there are additional sedimentary inputs to the more proximal coring sites in the Lake Linné (H, D, and C), however, as the sites are within the same catchment (Snyder *et al.*, 2000). The common stratigraphy of the four sedimentary archives (site H, D, and C) thus makes it possible to use the correlation between TOC RE and TOC HYP of core LDB13_I as a transfer function in order to reconstruct the TOC on the other archives by using only the hyperspectral data. The fossil OM content of the proximal cores is thus reconstructed at high resolution (figure 8).

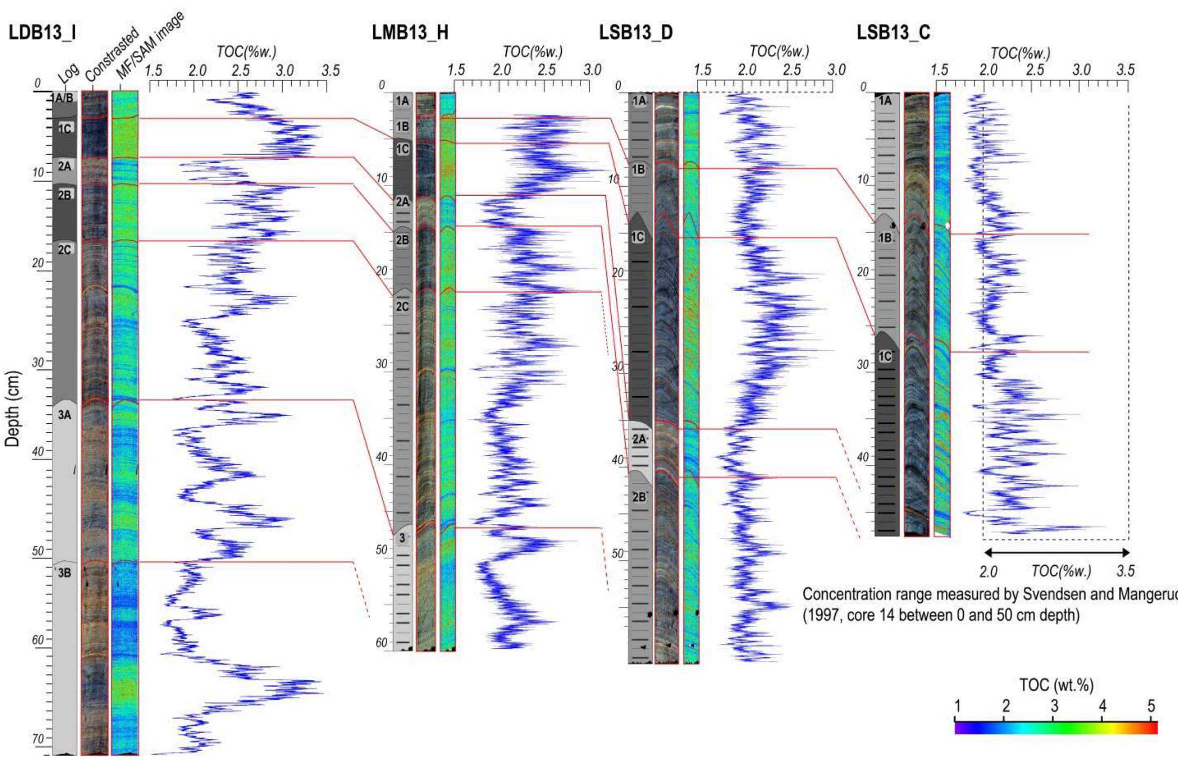

Figure 8: *TOC infer with the hyperspectral data on the four cores of the Lake Linné*

The TOC profiles are consistent with the sedimentary units identified in the different archives (see 4.1). For example, unit 1C, which has the highest TOC concentrations in core LDB13_I, also has the highest TOC values in the other three cores. Unit 2A has the lowest concentrations (<1.5% TOC). These differences are diluted in the more proximal archives where the TOC concentrations show significant variations that correspond to the stratigraphic resolution of the lamina (Figure 8). Previous cores were collected from Lake Linné and published by Svendsen and Mangerud in 1997. One of these cores is located near the coring location at Site C (core 14). The TOC of core number “14” in the top 50 cm oscillates between 2 and 3.5%. The values of TOC HYP in the LSB13_C archive are between 2 and 3 TOC% m and therefore in agreement with the values reported by Svendsen and Mangerud (1997). In addition, the TOC HYP of the thickest laminae attributed to the inflow of river sediments in unit 2C by the "with field samples" classification is estimated at 2% TOC HYP. This corresponds to the TOC RE measurements made on the river sediment samples (02_LowerLinnéElvaSed: 2.17% m and 05_MidLinnéElvaSed 2.57% m, figure 4a) thus reinforcing the power of the hyperspectral camera to reconstruct total organic carbon at high resolution.

5 Conclusion

The objective of this research is to test the application of hyperspectral imagery to 1) track sedimentary sources in a lacustrine archive using a source-to-sink approach and 2) to reconstruct total organic carbon concentrations based on the spectral signature of the lake sediments. To accomplish the first goal, two methods were used in order to identify the origin of the sedimentary material in a sediment core from Lake Linné. Approach A relies on samples retrieved from the lake watershed to identify specific sedimentary sources. The second method is based purely on pole extraction and excluded any field samples. Broadly, it appears that the end-member extraction (i.e. PPI method, Approach B) makes unnecessary the field samples for source-to-sink studies. Nevertheless, secondary sediment sources (intermediate storage, etc.), resulting from the mixture of two sources, are not detected by this method but are identified using the field sample calibration approach. It is therefore possible to produce a high-resolution image of the archive according to the origin of the sediments on the watershed (figure 5C). In the case of the Lake Linné, the application of hyperspectral imaging produces a high-resolution image that identifies the two major sedimentary inputs: the Linnébreen glacier in the South and the LIA cirque in the West.

The second part of this study aims at reconstructing TOC concentrations downcore at a high-resolution based on the spectral signature of organic matter calibrated with direct TOC measurements. The strong correlation between TOC measured with Rock-Eval pyrolysis and the hyperspectral index of OM in the core LDB13_I allows to establish a transfer function to quantify TOC in the other cores in a non-destructive way. This technical advantage allows to analyse several cores at low costs. The hyperspectral index is transform into concentration of organic carbon, which permits to compare the TOC concentration reconstructed in the proximal core LSB13_C with the concentrations published in former studies. This comparison shows that the reconstructed TOC with hyperspectral imagery compares favourably with previously published work (Svendsen and Mangerud, 1997). Moreover, the calibration of hyperspectral data enhances the resolution of TOC concentration beyond the maximum resolution of destructives analysis. The application of the transfer function allows to increase the quantity of information outcoming from the expensive and time consuming destructive analysis. This study shows the possibility to benefits with the combination of a low resolution, destructive but quantitative analysis and the strengths of a high-resolution, non-destructive but non-quantitative technique. Hyperspectral imaging is a promising tool for high-resolution proxy reconstructions as the acquisition process is fast and inexpensive with regard to the amount of data produced. These new technical features can add value to reconstructions with high resolution proxies across multiple sedimentary archives.

Acknowledgements

Authors are gratefull to National Science Foundation, Arctic Natural Sciences, Bill Wiseman Program Manager and faculty and staff of the Arctic Geology Department of UNIS

(University Centre in Svalbard). Analyses and A. Van Exem grant was funded by the Region Normandie, which supports the scientific consortium SCALE UMR CNRS 3730. This work was supported by public funds received in the framework of GEOSUD, a project (ANR-10-EQPX-20) of the program "Investissements d'Avenir" managed by the French National Research Agency.

Bibliography:

Arnaud, F., et al. (2016) ‘Erosion under climate and human pressures: An alpine lake sediment perspective’, Quaternary Science Reviews, 152, pp. 1–18. doi: 10.1016/j.quascirev.2016.09.018.

Bakke, J., et al. (2013) ‘Numerical analyses of a multi-proxy data set from a distal glacier-fed lake, Sørsendalsvatn, western Norway’, Quaternary Science Reviews. Elsevier Ltd, 73, pp. 182–195. doi: 10.1016/j.quascirev.2013.05.003.

Boardman, J. W. (1994) ‘Geometric mixture analysis of imaging spectrometry data’, Geoscience and Remote Sensing Symposium, 1994. IGARSS ’94. Surface and Atmospheric Remote Sensing: Technologies, Data Analysis and Interpretation., International, 4, pp. 2369–2371. doi: doi:10.1109/IGARSS.1994.399740.

Bonneau, L., et al. (2016) ‘Glacial erosion dynamics in a small mountainous watershed (Southern French Alps): A source-to-sink approach’, Earth and Planetary Science Letters. Elsevier B.V., 1. doi: 10.1016/j.epsl.2016.11.004.

Borruel-Abadía, V., et al. (2015) ‘Late Pleistocene to Holocene palaeoenvironmental variability in the north-west Spanish mountains: Insights from a source-to-sink environmental magnetic study of Lake Sanabria’, Journal of Quaternary Science, 30(3), pp. 222–234. doi: 10.1002/jqs.2773.

Boyum, J., and A. Kjensmo (1978) ‘Physiography of Lake Linnévatn, Western Spitsbergen’. Verhandlungen des Internationalen Verein Limnologie, p. v: 20, pp 609-615.

Briner, J. P., et al. (2016) ‘Holocene climate change in Arctic Canada and Greenland’, Quaternary Science Reviews, 147, pp. 340–364. doi: 10.1016/j.quascirev.2016.02.010.

Brosinsky, A., S. Foerster, K. Segl, J. A. López-Tarazón, et al. (2014) 'Spectral fingerprinting: characterizing suspended sediment sources by the use of VNIR-SWIR spectral information', Journal of Soils and Sediments. doi: 10.1007/s11368-014-0927-z.

Brosinsky, A., S. Foerster, K. Segl, and H. Kaufmann (2014) 'Spectral fingerprinting: sediment source discrimination and contribution modelling of artificial mixtures based on VNIR-SWIR spectral properties', Journal of Soils and Sediments, 14(12), pp. 1949–1964. doi: 10.1007/s11368-014-0925-1.

Butz, C., et al. (2015) 'Hyperspectral imaging spectroscopy: a promising method for the biogeochemical analysis of lake sediments', Journal of Applied Remote Sensing, 9(1), p. 96031. doi: 10.1117/1.jrs.9.096031.

Butz, C., et al. (2016) 'Sedimentary Bacteriopheophytin a as an indicator of meromixis in varved lake sediments of Lake Jaczno, north-east Poland, CE 1891???2010', Global and Planetary Change. Elsevier B.V., 144, pp. 109–118. doi: 10.1016/j.gloplacha.2016.07.012.

Clark, R. N. Swayze, G. A. Wise, R. Livo, K. E. Hoefen, T. M. Kokaly, R. F. and Sutley, S. J. 2007, USGS Digital Spectral Library splib06a, U.S. Geological Survey, Data Series 231

Cloutis, E. a., et al. (1990) 'Reflectance spectra of "featureless" materials and the surface mineralogies of M- and E-class asteroids', 95, pp. 281–293. doi: 10.1029/JB095iB01p00281.

Cloutis, E. A. (2003) 'Quantitative characterization of coal properties using bidirectional diffuse reflectance spectroscopy', Fuel, 82(18), pp. 2239–2254. doi: 10.1016/S0016-2361(03)00209-6.

Copard, Y., et al. (2006) 'Using Rock-Eval 6 pyrolysis for tracking fossil organic carbon in modern environments: Implications for the roles of erosion and weathering', Earth Surface Processes and Landforms, 31(2), pp. 135–153. doi: 10.1002/esp.1319.

Crassard, R., et al. (2013) 'Middle Palaeolithic and Neolithic Occupations around Mundafan Palaeolake, Saudi Arabia: Implications for Climate Change and Human Dispersals', PLoS ONE, 8(7). doi: 10.1371/journal.pone.0069665.

Dallman, W.K. 1992. Geological mad, Svalbard 1:100 000. Map n°16. B9G Isjfjorden, *Norsk Palarinstitut.*

Dearing, J. A., et al. (2010) ‘Complex land systems: The need for long time perspectives to assess their future’, Ecology and Society, 15(4). doi: 21.

Deaton, B. C., and W. Balsam (1991) ‘Visible spectroscopy: a rapid method for determining hematite and georthite concentration in geological materials’, Journal of Sedimentary Research, 61(October 1990), pp. 628–632.

De Wet, G. A., et al. (2017) ‘Holocene glacier activity reconstructed from proglacial lake Gjøavatnet on Amsterdamøya, NW Svalbard’, Quaternary Science Reviews. doi: 10.1016/j.quascirev.2017.03.018.

Di-Giovanni, C., et al. (1998) ‘Geochemical characterization of soil organic matter and variability of a postglacial detrital organic supply (Chaillexon Lake, France)’, Earth Surface Processes and Landforms, 23(12), pp. 1057–1069. doi: 10.1002/(SICI)1096-9837(199812)23:12<1057::AID-ESP921>3.0.CO;2-H.

Disnar, J. R., et al. (2003) ‘Soil organic matter (SOM) characterization by Rock - Eval pyrolysis : scope and limitations’, 34, pp. 327–343.

Gogolek, W., and W. Lewandowski (1980) ‘Preliminary geomorphological characteristic of Linnédalen (Spitsbergen , Svalbard Archipelago)’, Polar Polish Research, 1(4), pp. 7–19.

Hjelle, A., Lauritzen, O., Salvigsen, O. and Winsnes' T. S., 1986. Geological map. Svalbard 1:100.000. Sheet B10G Van Mijenfjorden. Nor. Polarins't. Temakart No. 2.

Horng, C. S., and C. A. Huh (2011) ‘Magnetic properties as tracers for source-to-sink dispersal of sediments: A case study in the Taiwan Strait’, Earth and Planetary Science Letters. Elsevier B.V., 309(1–2), pp. 141–152. doi: 10.1016/j.epsl.2011.07.002.

IPCC, 2013: Climate Change 2013: The Physical Science Basis. Contribution of Working Group I to the Fifth Assessment Report of the Intergovernmental Panel on Climate Change [Stocker, T.F., D. Qin, G.-K. Plattner, M. Tignor, S.K. Allen, J. Boschung, A. Nauels, Y. Xia, V. Bex and P.M. Midgley (eds.)]. Cambridge University Press, Cambridge, United Kingdom and New York, NY, USA, 1535 pp.

Jenny, J. P., et al. (2014) ‘A 4D sedimentological approach to reconstructing the flood frequency and intensity of the Rhône River (Lake Bourget, NW European Alps)’, Journal of Paleolimnology, 51(4), pp. 469–483. doi: 10.1007/s10933-014-9768-4.

Koiter, A. J., et al. (2013) ‘The behavioural characteristics of sediment properties and their implications for sediment fingerprinting as an approach for identifying sediment sources in river basins', Earth-Science Reviews. Elsevier B.V., 125, pp. 24–42. doi: 10.1016/j.earscirev.2013.05.009.

Kruse, F. A., et al. (1993) 'The spectral image processing system (SIPS)—interactive visualization and analysis of imaging spectrometer data', Remote Sensing of Environment, 44(2–3), pp. 145–163. doi: 10.1016/0034-4257(93)90013-N.

Lafargue, E., et al. (1998) 'Rock-Eval 6 Applications in Hydrocarbon Exploration, Production, and Soil Contamination Studies', Oil & Gas Science and Technology, 53(4), pp. 421–437. doi: 10.2516/ogst:1998036.

Leithold, E. L., et al. (2016) 'Source-to-sink sedimentary systems and global carbon burial: A river runs through it', Earth-Science Reviews. Elsevier B.V., 153, pp. 30–42. doi: 10.1016/j.earscirev.2015.10.011.

Mangerud, J. A. N., and J. I. Svendsen (1989) 'Deglaciation chronology inferred from marine sediments in a proglacial lake basin, western Spitsbergen, Svalbard', 1986.

Milliken, R., and J. Mustard (2007) 'Estimating the water content of hydrated minerals using reflectance spectroscopyII. Effects of particle size', Icarus, 189(2), pp. 574–588. doi: 10.1016/j.icarus.2006.12.028.

Milliman, J. D., and J. P. M. Syvitski (1992) 'Geomorphic / Tectonic Control of Sediment Discharge to the Ocean : The Importance of Small Mountainous Rivers Author (s): John D . Milliman and James P . M . Syvitski Published by : The University of Chicago Press Stable URL : http://www.jstor.org/stabl', 100(5), pp. 525–544.

Nesje, A., et al. (2001) 'Holocene glacier fluctuations of Flatebreen and winter-precipitation changes in the Jostedalsbreen region, western Norvay, based on glaciolacustrine sediment records', The Holocene, 11(3), pp. 267–280. doi: 10.1191/095968301669980885.

Noel, H. (2001) 'Caractérisation et calibration des flux organiques sédimentaires dérivant du bassin versant et de la production aquatique (Annecy, le Petit Lac) : rôles respectifs de l'Homme et du climat sur l'évolution des flux organiques au cours des 6000 dernières années'. Thèse de doctorat en Sciences de l'univers. Pétrographie et géochimie organiques. Université d'Orléan. Dir. Lallier-Vergès, E.

Owens, P. N., et al. (2016) 'Fingerprinting and tracing the sources of soils and sediments: Earth and ocean science, geoarchaeological, forensic, and human health applications', Earth-Science Reviews. Elsevier B.V., 162, pp. 1–23. doi: 10.1016/j.earscirev.2016.08.012.

PAGES 2k Consortium, 2013, Continental-scale temperature variability during the past two millennia, Nature Geoscience,6, pp. 339–346.

Pulley, S., et al. (2015) ‘The application of sediment fingerprinting to floodplain and lake sediment cores: assumptions and uncertainties evaluated through case studies in the Nene Basin, UK’, Journal of Soils and Sediments, 15(10), pp. 2132–2154. doi: 10.1007/s11368-015-1136-0.

Resentini, A., et al. (2016) ‘Tracing erosion patterns in Taiwan by quantitative provenance and geomorphological analysis’, 18, p. 8084. doi: 10.1002/2016JF004026.

Reusche, M., et al. (2014) ‘10Be surface exposure ages on the late-Pleistocene and Holocene history of Linnébreen on Svalbard’, Quaternary Science Reviews. Elsevier Ltd, 89, pp. 5–12. doi: 10.1016/j.quascirev.2014.01.017.

Revel-Rolland, M., et al. (2005) ‘Sr and Nd isotopes as tracers of clastic sources in Lake Le Bourget sediment (NW Alps, France) during the Little Ice Age: Palaeohydrology implications’, Chemical Geology, 224(4), pp. 183–200. doi: 10.1016/j.chemgeo.2005.04.014.

Sandgren and Snowball (2001), in W. M. Last & J. P. Smol (eds.), 2001.Tracking Environmental Change Using Lake Sediments. Volume 2: Physical and Chemical Techniques. Thompson, R. & F. Oldfield, 1986. Environmental Magnetism. George Allen and Unwin, London, 227 pp.

Snyder, J. a., et al. (2000) ‘Holocene cirque glacier activity in western Spitsbergen, Svalbard: sediment records from proglacial Linnévatnet’, The Holocene, 10(5), pp. 555–563. doi: 10.1191/095968300667351697.

Svendsen, J. I., et al. (1987) ‘Postglacial marine and lacustrine sediments in Lake Linnévatnet, Svalbard’, Polar Research, 5(3), pp. 281–283. doi: 10.3402/polar.v5i3.6888.

Svendsen, J. I., and J. Mangerud (1997) ‘Holocene glacial and climatic variations on Spitsbergen, Svalbard’, The Holocene, 7(1), pp. 45–57. doi: 10.1177/095968369700700105.

Svendsen, J., and J. Mangerud (1992) ‘Paleoclimatic inferences from glacial fluctuations on Svalbard during the last 20 000 years’, Climate Dynamics, 6(3–4), pp. 213–220. doi: 10.1007/BF00193533.

Swart, N. (2017) ‘Climate variability: Natural causes of Arctic sea-ice loss’, Nature Climate Change. Nature Publishing Group. doi: 10.1038/nclimate3254.

Van Exem, A., et al. (2018) ‘Hyperspectral core logging for fire reconstruction studies’, Journal of Paleolimnology, 59(3), pp. 297–308. doi: 10.1007/s10933-017-0009-5.

Walsh, J. P., et al. (2016) ‘Source-to-sink research: Economy of the Earth’s surface and its strata’, Earth-Science Reviews, 153, pp. 1–6. doi: 10.1016/j.earscirev.2015.11.010.